Resistivity and Optical Transmittance Simulation on Metal Embedded Transparent Conducting Oxide Thin Films

by

Chia-Ling Fang

A Thesis Presented in Partial Fulfillment
of the Requirements for the Degree
Master of Science

Approved April 2012 by the
Graduate Supervisory Committee:

Terry Alford, Chair
David Theodore
Peter Crozier

ARIZONA STATE UNIVERSITY

May 2012

ABSTRACT

This work focuses on simulation of electrical resistivity and optical behaviors of thin films, where an Ag or Au thin layer is embedded in zinc oxide. Enhanced conductivity and transparency were earlier achieved with multilayer structured transparent conducting oxide (TCO) sandwich layer with metal (TCO/metal/TCO). Sputtering pattern of metal layer is simulated to obtain the morphology, covered area fraction, and the percolation strength. The resistivity as a function of the metal layer thickness fits the modeled trend of covered area fraction beyond the percolation threshold. This result not only presents the robustness of the simulation, but also demonstrates the influence of metal morphology in multilayer structure. Effective medium coefficients are defined from the coverage and percolation strength to obtain simulated optical transmittance which matches experimental observation. The coherence of resistivity and optical transmittance validates the simulation of the sputtered pattern and the incorporation of percolation theory in the model.

DEDICATION

To my family

ACKNOWLEDGMENTS

I am heartily thankful to my advisor, Prof. Terry Alford, whose guidance from the initial to the final level enabled me to develop an understanding of the subject. This thesis would not have been possible without his support and confidence in me.

I would like to show my gratitude to Dr. David Theodore and Prof. Peter Crozier for being my committee members and taking time to review my work.

I am indebted to my lab mates, Rajitha Vemuri, Aritra Dhar, Sayanton Das, Pai Liu, Shengke Zhang and Hyung Woo Choi, for the inspiration and support that they have provided. Many thanks to my dear friends for their company and encouragement, even some are far apart.

Finally, I would like to thank my parents who warm my heart with their eternal love, my sister who always directs me to be a better person, and my nephew whose laugh is the joy in my hard time.

TABLE OF CONTENTS

Page

CHAPTER Page

LIST OF TABLES

LIST OF FIGURES

Chapter 1: INTRODUCTION

1.1. Transparent Conducting Oxides

Transparent Conducting Oxides (TCOs) have attracted lots of attention due to their transparency in visible region, metallic conductance and along with wide range of applications in industry. For photosensitive electronic devices, TCOs are essential components acting as transparent electrical contacts or electrodes in flat panel displays, touch screens, thin film solar cells, and electrochromic devices [1-4]. Many researches are dedicated to improve the quality of TCOs for specific requirements depending on the targeted application. Generally, a certain sheet resistance is needed in order to meet the electrical functionality. The range of sheet resistances is from the order of 400–700 Ω/sq required for electrodes in touch screens to below 10 Ω/sq for large area flat panel displays and thin film solar cells [5]. Another important property is the transmittance of the layers in the spectral range of interest. This range can be determined by the sensitivity of human eyes, the efficiency of the absorber material for solar cells, or the emission spectra of the active materials used for new lightening technologies[2].

The most popular TCOs are tin-doped indium oxide (ITO), fluorine-doped tin oxide, and aluminum-doped zinc oxide. ITO has low electrical resistivity, $2x10^{-4}$ Ω cm at deposition temperature above 250 ℃, and intrinsic band gap 3.7 eV. However, Indium is a scarce metal which has increasing demand and also market value. Among all of potential ITO substitutions, a TCO/Metal/TCO sandwich structure is proposed to meet desired properties and to reduce demands on indium. This multilayer structure is proved to have competent quality because the metal interlayer allows one to decrease the overall resistivity even though the TCO electrical quality is not optimum [6].

Besides of resistivity, the choice of substrates also plays an important role in deciding proper TCOs. The major production of flat panel displays and thin film solar cells is based on glass substrates which provide rigid support and can stand the high temperature in manufacturing process. However, it is necessary to replace rigid glass with flexible plastics in order to meet the expectation for growing renewable energy and electronic markets with low prices. It is easier to handle the thickness of polymer foils which can vary from tens to hundreds of micrometers. One issue arises in replacing. That is, polymer foils are relatively unstable in high temperature which is required in process. TCO/Metal/TCO demonstrates its another advantage in achieving good quality under low process temperature and becomes a good substitution of TCO single layer [7]. The TCO/metal/TCO electrodes have been applied to organic luminescent displays and organic photovoltaic devices [7, 8], also in inorganic liquid crystal displays, flexible random access memories, capacitors, gas sensors, and dye-sensitized solar cells [6].

1.2. TCO/Metal/TCO Thin Films

As a solution in material scarcity and substrate heating, TCO/Metal/TCO thin films are widely studied in its ability on flexible and low-cost plastic substrates such as polyethylene terephthalate (PET) and polyethylene naphthalate (PEN).

Metal layer is the key element in determining the sheet resistance of the TCO/metal/TCO structure. Ag is the first choice for the metal interlayer due to its low resistivity comparing to other metals, followed by Cu that has an only slightly higher value. However, for metal thin films, the transmittance and the sheet resistance change rapidly with layer thickness. Due to a transition from a continuous film to one composed of distinct islands of metal atoms, properties differ considerably from the bulk metal. In general, the critical thickness for this transition depends on the substrate and deposition conditions in addition to the specific metal.

1.3. Objective

As increasing attention paid on TCO/Metal/TCO multilayer structure, it is essential to understand how metal interlayer results resistivity improvement. Due to the lower optical transmittance of metal thin films than pure TCO, the resistivity and the transmittance need to compromise for each other as increasing metal layer thickness. In order to determine a critical thickness of metal layer, a comprehensive understanding in metal layer morphology will assist the discussion of resistivity and optical transmittance.

However, most of embedded metals are not able to be seen by present instruments. A lack of study in this field makes experimental results have no path to follow. We therefore want to combine a surface morphology simulation and percolation concept to describe the resistivity and optical transmittance for different metal thickness in the multilayer structure. With this new view point, one should be able to not only fit previous experimental results, but also predict the critical metal thickness that results morphology transition of metal and resistivity transition of the whole sandwich structure.

1.4. Summary

To simplify the system in discussion, we focus on ZnO/Ag/ZnO and ZnO/Au/ZnO which both have complete experimental results done by previous members in our research group [9, 10]. Both of the cases were using magnetron sputtering due to its advantages in ease of large-area-deposition, low deposition temperature, high deposition rate, good adhesion on substrate, good uniformity and simple equipment. The similarity in materials and deposition method makes the comparison easier.

A metal surface simulation will be demonstrated in chapter 2. This simulation provides the morphology change of the metal interlayer, including particle distribution, covered area fraction and percolation phenomena. Basing on the percolation phenomena, we propose the resistivity change with metal thickness should be dominated by the percolating morphology of the metal layer. A discussion of percolation theory, critical thickness prediction and data fitting are contained in chapter 3. Optical transmittance also gives evidence in supporting our model. We will introduce Bergman effective medium model in order to calculate optical transmittance in chapter 4. Bergman model also uses percolation concept to describe the optical properties of discontinuous metal layer. With simulated resistivity and optical transmittance, we are able to find the largest Haacke figure of merit which points out 9 nm metal interlayer is the best thickness for solar applications. The conclusion will be addressed in chapter 5.

Chapter 2: METAL SURFACE SIMULATION

2.1. Introduction

Due to the low resistivity of metal, great improvement in resistivity has been observed in dielectric-metal-dielectric multilayer structure. It is obvious that the more metal is embedded the lower resistivity can be performed. However, in order to keep the advantage of transparent conducting oxide, a thinner metal layer is preferred to retain the transparency. Fortunately, a few nanometer metal thin layer already provides acceptable resistivity which is more than four orders lower than pure oxides and also thin enough to allow light transmission [11]. In this thickness, metal layer is so thin that islands appear instead of continuous and homogeneous film. Therefore, the morphology of these islands should dominate the conduction mechanism. Also, possible optical resonance on metal should be taken into consideration [12-14]. In pursuing a balance between transparency and resistivity, we need to have a full understanding in the metal thin layer, including morphology, conduction mechanism and effects in transmittance.

Although scanning electron microscope (SEM) and atomic force microscopy (AFM) can provide good images of metal islands, strong dependence of manual analysis, including counting islands and measuring spacing between islands, makes the extracted parameters unreliable and inaccurate [15]. Moreover, for the whole multilayer structure, it is hard to have metal only images. To overcome these problems, we simulate metal deposition and perform a simulated metal surface with reasonable extracted parameters. Comparing images and our model, one can obtain a clear view of metal layer, especially

on its dependence of deposition time and thickness. It will be easy to adjust simulation parameters for different materials or deposition methods.

In this chapter, the concept of our simulation and how to connect simulation results to experimental observation will be described. A discussion in the formation of a continuous metal film from discontinuous islands will also demonstrate the reliability of our simulation.

2.2. Sputtered pattern simulation

2.2.1. Metal Island Growth

Depending on deposition rate, metal islands on a flat substrate will grow into uniform thin film under different paths. Under low deposition rate, one can imagine atoms attach to the substrate one by one. The very first atom has high mobility to walk randomly on the substrate, as does the second atom. It is highly possible that two atoms meet and form a larger island which has lower mobility. This island will then meet the consequent atoms and keep increasing size and decreasing mobility. Slow deposition machine, such as molecular beam epitaxy, can produce films with large grains. However, in our case, sputter deposition is used, causing many isolated atoms present before migration or large islands form. Atoms bond to neighbors before they migrate to a distant island. Also, consider adatom-adatom interaction; metals themselves have stronger bonding energy than the one between metal and amorphous oxide. Therefore, it is more possible that metal grows under Volmer-Weber (V-W) growth mode [16]. V-W mode described thin film growth starts from islands formation. Even when thickness of thin film is larger than one monolayer, islands are preferred to be the main morphology.

For our few nanometer metal thin layer, two stages of formation has been proposed [9]. In the beginning, as the deposition time increases the number of islands also increases, but no obvious coalescence shows up until stage two. During this period, island formation follows V-W mode. In the second stage, islands are dense and able to coalesce with others to decrease their surface potential. A detailed discussion and another stage of formation will be performed by comparing real sample images and simulation results.

2.2.2. Simulation concept

We make two straight forward assumptions in sputtering mechanism. First, for a given time interval, the same amount of metals will be sputtered onto the substrate. Second, those metals are randomly distributed clusters having the same size. That is, for a certain area, there is a possibility *(p)* to be occupied by a certain amount of metal. As the sputtering time increasing to two time intervals, another randomly distributed deposition layer with the same *p* will overlap on the first deposition result. Therefore, increasing sputtering time is proportional to increasing the number of passed layers.

To achieve this layer-by-layer simulation, we generate an *L* square array to represent each pass in which each site position has the same possibility *(p)* to be occupied. Then, we take the integral of the results for several passes where each has the same occupied possibility but randomly distributed occupied positions. A schematic figure presents this concept (figure 2.1.A). Figures 2.1.B, C, and D demonstrate integral results of one, two and three passed layers, respectively. It can be observed that some positions have surrounding neighbors and some do not. Neighbors are defined as those that connect with each other only 1 site from the top, bottom, left and right. In figure 2.1.E, different colors indicate different isolated islands. It should be noticed that each island has different shapes and distances to other islands. This two results play important roles in conduction mechanism and will be discussed later.

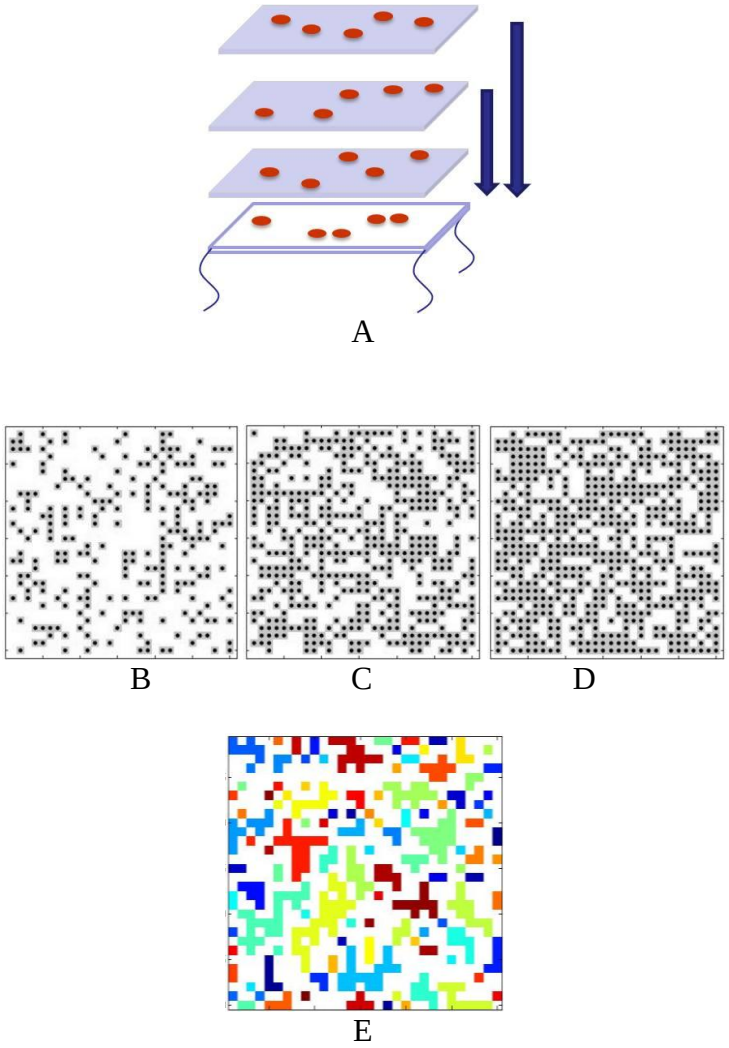

Figure 2.1. Illustration of simulation concept (A) and occupied sites for the integral of different number of passed layers (B-E): In A, layer-by-layer deposition concept shows adding number of passed layers with different distribution of occupied sites. B, C, and D demonstrates the increase of occupied sites with 1, 2 and 3 number of passes, respectively. E uses different colors to indicate different isolated islands.

To build the sputtered pattern in 3-D, we need to determine its shape and volume. Although many different shapes of sputtered metal clusters are possible, a hemisphere is one of the most possible and easy to define shapes. Therefore, in our simulation, we apply a hemisphere to represent sputtered metal clusters. A hemisphere replaces and is centered at an occupied position of previous discussion. The radius of this hemisphere is the distance between two array points (1 unit). This simulation enhances the overlapped areas between two adjoined occupied positions which matches our expectation that adjoined metal clusters prefer to aggregate for decreasing surface potential.

Our simulation code is built on Matlab R2011, distributed by the MathWorks company. Program flow starts from assigning a size *(L)* for an array. An *L x L* array will be created and each site in this array has a random number between 0 and 1, which is generated by Matlab's built-in random number generator. By choosing a desired probability *p*, all sites with a random number smaller than *p* are kept and their positions are also recorded as coordinates on an *x-y* plane where hemispheres with a radius of 1 are located on recorded positions. Adjusting *p* allows us to determine the desired density of occupied positions in each pass. Depending on the random numbers generated each time, the actual recorded positions will be different. For another pass, a new *L x L* array is created with different random numbers and recorded positions. By adding two layers together, we can say it represents the deposition results for two time intervals. Our simulation uses a start-from-beginning calculation. That is, to obtain the integral results of three passes and five passes separately, it will generate three arrays and another five

new arrays instead of simply adding the result of two passes on the one of three passes. In this way, we can have more general distribution without a strong dependence on previous results.

The 3-D layer-by-layer deposition result is performed and shown in figure 2.2 A (array size: 15, probability: 0.1, number of passes: 2) Another parameter, contour value, is introduced here to increase the flexibility of our surface simulation. As discussed above, metal clusters will reshape themselves to achieve the lowest surface potential. Therefore, a little edge shrinking should be expected to match a practical situation. The contour value *c* is a variable parameter that can be used to determine the top contour view of vertical height. By changing the *c* value, one can emphasize on his/her expecting phenomena. For example, a lower *c* will generate a surface with clusters widely spread. On the other hand, a higher *c* corresponds to a surface which contains clusters with smaller radiuses and emphasizes the threshold for the appearance of large-area coalescence. Therefore, in a low *c* case, the coverage is relatively large for the first few passes, but for the integral coverage of a large number of passes increasing rate of the coverage slows down. Figure 2.2 B demonstrates the contour plot of figure 2.2 A with c=0.5. We will define islands and calculate areal coverage and distances between islands based on this type of contour plots.

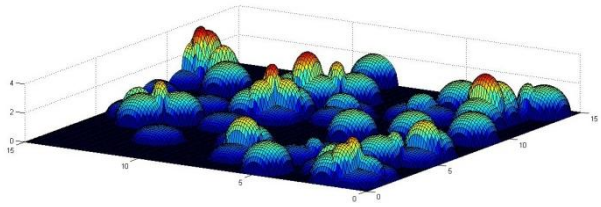

A

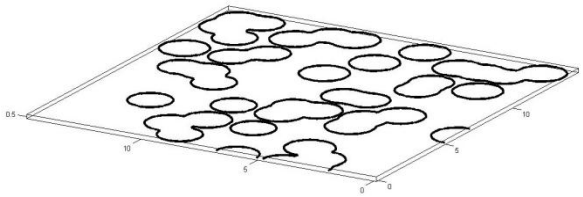

B

Figure 2.2 Topography and morphology simulation. A is a 3-D layer-by-layer deposition result (array size:15; probability:0.1; number of layers:2). B is a 2-D contour plot of A (contour height=0.5)

2.3. Results and sample images

We use “coverage” here to represent the total covered area fraction in our simulation. Because we set a contour value, we are able to consider the edge-shrinking effect and focus on large island formation. However, the coverage becomes different from simply calculating the probability of appearance. We need to count the whole covered area on the contour plot. Three curves in figure 2.3 demonstrate the influence of different *p, c* to the total coverage. The *p* value dominates the increasing rate of coverage as the number of passes increases. The *c* value mainly controls the total coverage in the first few passes.

The solid curve in figure 2.4 A is the simulated coverage change with increasing number of passes for p=0.1 and c=0.5. The tendency is similar to a second order polynomial starting from 0 and getting close to 1 when the number of passes is larger than 6. For real samples, we can also obtain coverage extracted from SEM images of bare metals on oxides. Figure 2.4 B is a series of images of Ag on the top of ZnO. The Ag layer is not covered by another layer of ZnO. The ZnO is sputtered at 10 mTorr argon pressure using 100 W RF power. Ag is deposited using 10 mTorr argon pressure and 40 W DC power. The thickness labeled on figures are determined by Rutherford Backscattering Spectrometry. The coverage is analyzed in ImageJ. Rough analysis of coverage indicates the covered areal fractions are 0.39, 0.64, 0.82, 0.92 for 2nm, 4nm, 6nm, 8nm Ag layer, respectively. Accuracy is influenced by manual color threshold control and image contrast. As can be seen on images, there are wrinkles on Polyethylene Naphthalate (PEN) substrates. Because PEN is one type of polymer, heating during sputtering and SEM scanning may result in agglomeration of polymers and destroy the smooth surface.

By comparing the coverage extracted from images to simulation results, we see the coverage of 2 nm, 4 nm, 6 nm and 8 nm match the simulated coverage for number of passes 2, 4, 6 and 8, respectively. This discrete mapping not only supports our layer-by-layer growth assumption, but also gives a clue in connecting real samples and the virtual number of passes. Therefore, we are able to tune the *p* and *c* values for a better fitting to the real coverage change. Our goal is to build a surface to describe statistical behaviors and minimize number of samples prepared. Even though simulated patterns are not exactly the same as observation, the continuous curves describe overall behaviors which are close to the observation.

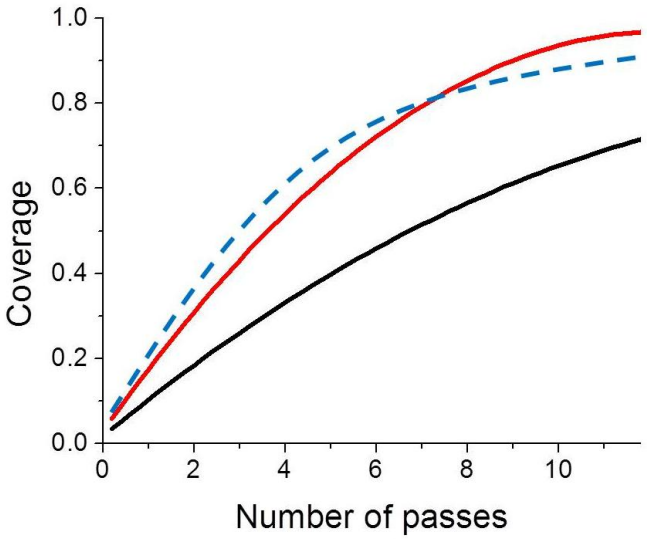

Figure 2.3. Coverage comparison with respect to different occupant probability (*p*) and contour height (*c*).
For red solid line, the *p* equals to 0.08 and *c* is 0.5. Black solid line has lower *p* (0.04) and the same *c* (0.5) as red one. A slower increasing with respect to number of passes is observed and indicates probability dominates coverage increasing rate. Blue dashed line has the same *p* (0.08) as red solid line but lower *c* (0.1). Higher increasing rate in the first few number of passes but small increase for larger number of passes are due to little emphasis on overlapping phenomenon for small contour height value.

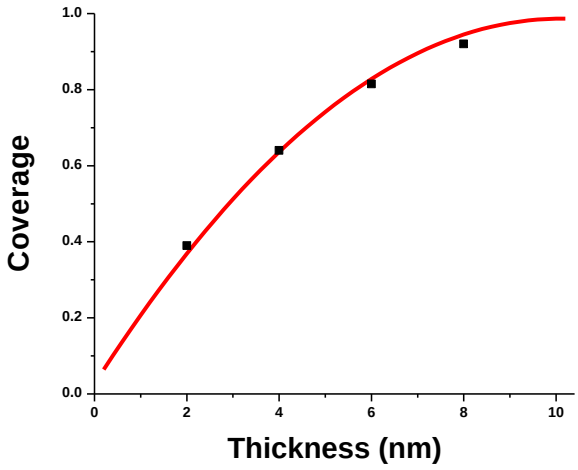

A

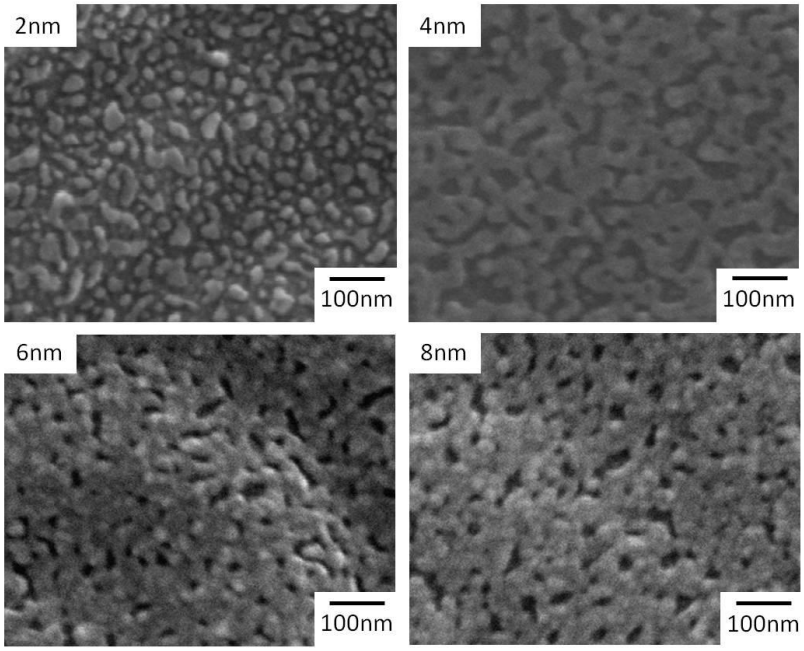

B

Figure 2.4. Coverage prediction and SEM picture comparison. A has a predicted coverage in solid line and four shaded squares (■) representing coverage extracted from SEM pictures shown in B. B contains four SEM pictures with different metal thickness: Above left, 2 nm; above right, 4 nm; below left, 6 nm; below right, 8 nm.

As described in Metal Island Growth section, we expect to find nearest distances between islands continuously decrease due to more islands formation. However, our simulation results show that after first decreasing an increase of spacing ensues (figure 2.5.) In the same figure, one can observe the number of islands increases at the beginning and turns to decrease at the same time island spacing increases. This explained what exactly happens when coalescence starts to dominate surface morphology. In the beginning of deposition, the number of islands increases while space is filled by small islands, so their spacing decreases. However, as islands start to coalescence with nearest neighbors, the number of islands is less and large spacing is left. Then, we observe the averaged spacing increases. Further coalescence and coarsening result in continuously decrease in both the number of islands and their spacing as expected. The turn point presents evidence in large scale coalescence. Reasonable explanation indicates the robustness of our simulation that can predict and describe real morphology change.

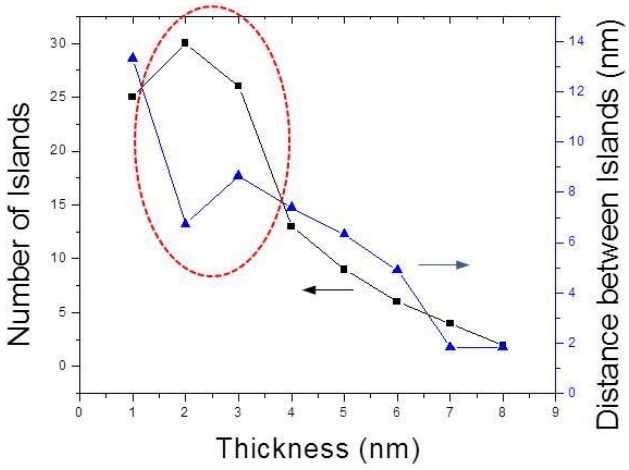

Figure 2.5. Predicted number of islands per unit area and average distance between islands. Linked black shaded squares (-■-) represent the number of islands change with increase of metal layer thickness. Blue shaded triangles (-▲-) denote the distance between islands change with increase of metal layer thickness. Red dashed circle points out unexpected change which is closer to real observation.

2.4 Summary

Details of the algorithm of our simulation are given in this chapter. Discussions also show the reasonableness and the reliability of our simulation. It should be noticed that we have two parameters *p* and *c* which can be obtained by considering extracted information from image analysis and comparing with different material. Simulation results give us distances between islands and coverage change with thickness. In later chapters, simulation results will be used to explain the resistivity variation and to determine effective medium coefficient in describing optical behaviors.

Chapter 3: RESISTIVITY WITH PERCOLATION THEORY

3.1 Introduction

Transparent conducting oxide (TCO) embedded with metal thin layer has been widely studied because of their specialty. Great improvement of conductivity but elimination of transparency with increasing metal layer thickness make it extremely important to find a critical thickness of the metal layer that has low resistivity but remains qualified transparency. In order to gain insight on this issue, we focus on the dielectric-metal-dielectric stacks which were fabricated, measured and reported previously from our group. As described in chapter 1, zinc oxide has great potential as a commercial TCO material, and noble metals, Au and Ag, are proposed to be most suitable due to their optical performance. In this chapter, we will demonstrate how our simulation results predict and fit experimental results by using the concept of percolation.

3.1.1. Sample discussion and Resistivity model

There are two types of sample in our discussion. First, we look into variation of resistivity of ZnO/Ag/ZnO and then migrate to ZnO/Au/ZnO as a further proof for the robustness of our simulation.

As a consequent study of previous experimental results, we follow the same fabrication procedure and conditions [9, 10]. Both ZnO/Ag/ZnO and ZnO/Au/ZnO samples are deposited on flexible substrate polyethylene naphthalate (PEN) for potential studies on flexible display.

Details of fabrication can be found in previous reports [9,10], partial information is provided here for better understanding of sample structure. The base pressure prior to deposition was approximately $1x10^{-7}$ Torr. The ZnO was sputtered at 10 mTorr argon pressure using 100 W RF power. Silver and Gold were deposited using 10 mTorr argon pressure and 40 W DC power. There was no break in vacuum at any stage during the preparation of the films. Both top and bottom ZnO layers were approximately 30 nm thick. The Ag thicknesses were varied between 8 nm and 14 nm, Au thicknesses were varied between 1 nm and 12 nm. Schemes in figure 3.1 A show the construction of two different stacks.

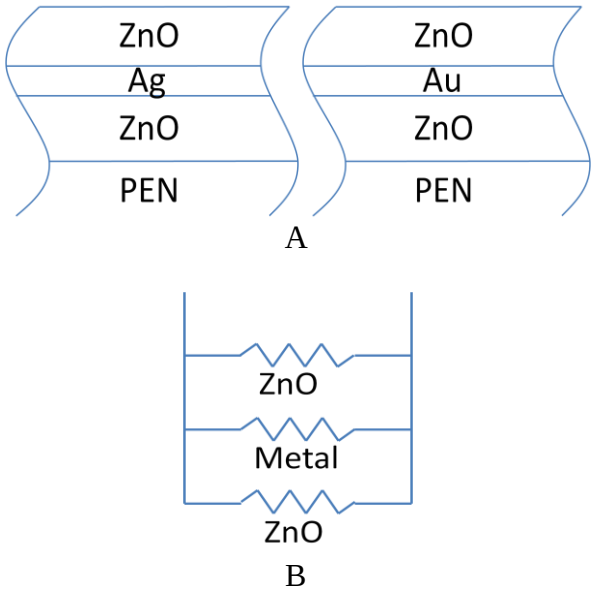

Figure 3.1. Illustration of two ZnO/Metal/ZnO and parallel resistor model. Left figure in A is ZnO/Ag/ZnO configuration; right figure in A is for ZnO/Au/ZnO. B has three resistors (two for ZnO and one for metal layer) connecting in parallel.

Figure 3.1.B schematically presents our model that the resistance of the top and bottom ZnO films are in parallel with the resistance from metal layer. This model is straight forward and reasonable in describing the dominant role in resistivity of each layer. However, in our observation, metal layer is filled by discontinuous islands, so bulk or thin film resistivity are both not applicable here. We propose a new view point by looking into the percolation phenomena of metal thin film. Using the simulation result of sputtered pattern from the last chapter, a fitted curve appears and shows critical metal thickness and resistivity change.

Figure 3.2.A and B show the change of resistivity of ZnO/Ag/ZnO and ZnO/Au/ZnO, respectively. From our group's previous experiments [9, 10], one can observe the resistivity drops at 8 nm Ag stack, but the lack of data points with metal thickness between 0 nm and 8 nm makes the critical drop point vague. More clear and dividable stages in ZnO/Au/ZnO indicate three possible stages: For 0 nm to 2 nm Au films, a slow decrease of resistivity implied a discontinuous film and its limitation in resistivity improvement. After that, a steep change in resistivity indicated metal thin film start to dominate the resistivity of the whole stack. What is happening during this transition is our main concern.

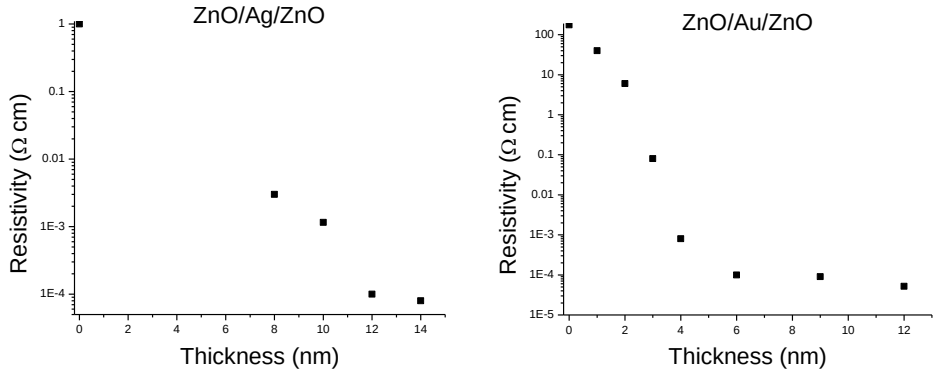

A B

Figure 3.2. Resistivity of ZnO/Ag/ZnO and ZnO/Au/ZnO versus metal layer thickness. A is for Ag embedded multilayer structure; B is for Au embedded structure.

3.1.2. Percolation theory

In observing metal island coalescence, we find a similar phenomena to percolation. Relative observation has also been reported [15]. Resistivity of thin metal film changes with annealing time and temperature were also related to percolation of metal morphology [17]. The importance of morphology gives us a hint and makes us question ourselves how the resistivity changes when the morphology is in transition, especially from isolated islands to uniform metal thin films. Here is an introduction of percolation as a preview of the concept which will be discussed later.

Percolation theory is usually applied to describe phase transition. With a given probability of occupancy for each site, adjoined sites form a cluster if they happened to be both occupied. Figure 3.3. shows the occupied sites when p=0.5 and p=0.6. Different isolated islands are colored with different colors. Arrows in both ends of one large cluster in figure 3.3. point out the appearance of an infinite cluster when p is large enough. Percolation threshold (p_c) is the critical probability that an infinite cluster may appear. If the probability is larger than p_c, there is at least one infinite cluster regarding to all sites. The value of p_c strongly depends on the dimension of sites, bonding type, and lattice structure. For an one dimensional lattice, percolation threshold is 1 which means all sites have to be occupied to form an infinite chain. For a 2-D square lattice, percolation threshold is about 0.593. Accuracy depends on the number of calculated sites.

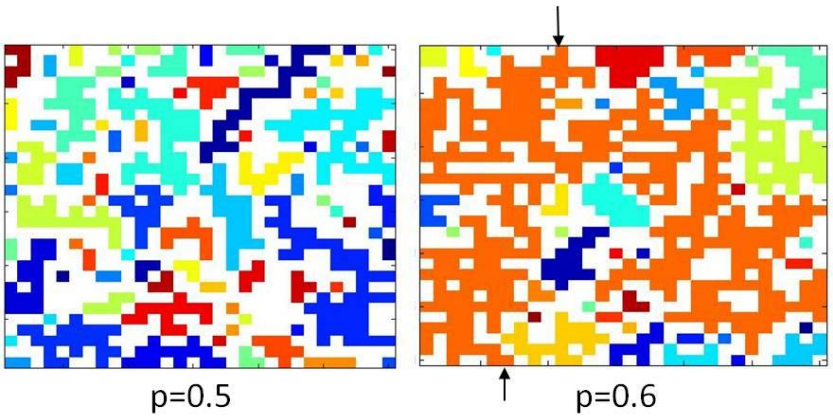

Figure 3.3. Illustration of occupied sites and clusters in different probability. Each color represents one cluster. Left picture has more small individual clusters than right one. An infinite path appears from one arrow to another in right picture.

The resistivity change with respect to two dimensional percolation was performed by Last and Thouless [18]. They punched holes to control the removed area of a conductive paper. Removing conductive area is the opposite direction from our case which adding more mass to form connection. The more removed areas caused lower conductivity. Their results indicated that a more rapid drop in conductivity occurs when the concentration of holes close to a threshold value. When the concentration of holes is lower than threshold, there are many paths for electrons to travel through. As closing to threshold, most paths are disconnected and lots of daggling paths on the rest of connected paths. Those daggling paths result in conductance rapid drop because even they present as paths but they have no contribution to the conductance. Once all paths are disconnected from one side of paper to the other side. It is called percolation threshold [18].

It is well known that conductivity has a relationship with occupancy probability as $\sigma \propto (p - p_c)^{\mu}$ [18] where p_c is the threshold probability and μ is the conductivity exponent.

In the case of no biased percolation disorder, μ equals to 1.299 [18]. However, the coalescence of metal islands in our case differs from simple percolation. The coalescence is mainly caused by the increase of deposited mass which makes both lateral and vertical growth. However, in observing percolation on our metal layer morphology, we only emphasize on lateral distribution. This emphasis diverges our model from unbiased situation. μ , therefore, in later resistivity discussion μ will be set as a free scaling parameter. Our goal is to find a certain deposition time (or thickness) that islands form large clusters and dominate the resistivity of the multilayer structure. Moreover, an interesting view point is to determine percolation strength which corresponds to how many sites are involved in infinite metal clusters on the surface. This percolation strength is an important parameter not only in resistivity calculation but also in optical effective medium coefficient calculation. Percolation strength *(P)* is defined as following

$$P = \frac{\text{Size of the percolating cluster}}{\text{Number of lattice sites}}$$

3.2 Metal thin film model

From the morphology of sputtered Ag on ZnO, we notice metal islands form first during a short sputtering time and then large scale of coalescence happens before continuous film appears. A continuous film can be referred to continuous paths for electron transmission. When the spacing between paths is filled, a continuous film becomes an uniform film. These phenomena indicate three stages instead of two in previous report [9]. Figure 3.4. divides this three stages into A, B and C schematic plots: A) Islands only; B) Percolating, may or may not reach threshold; and C) well-covered surface. For our interest of finding the decrease of resistivity, we focus on stage B, that is, when islands become large clusters and form conducting paths. In this stage, the surface contains some continuous paths but also some discontinuous islands. We need to take percolation strength into consideration.

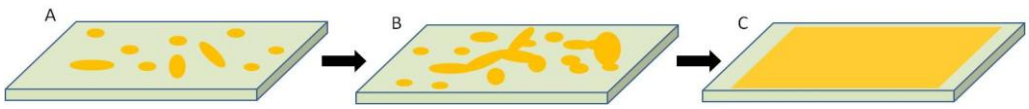

Figure 3.4. Illustration of metal morphology in different stages: In A stage, there are small islands only. In B stage, islands start to connect with each other and form larger conducting paths. In C stage, the surface is an uniform metal layer.

We start from our simulation. As described in chapter 2, we can have a sequence of surfaces denoting the results for a sequence of deposition time. The random array for defining possible metal location has dimensions of 50 x 50. The 3-D array for profiling metal hemisphere is 10 times larger with a step 0.1 between consequent integers. Figure 3.5. is a sequence of the morphology of deposition results, with probability p=0.1 and contour height c=0.5. Figure 3.4 A-H demonstrates the integral results of different number of passed layers from 1 to 8 as described in chapter 2. Table 3.1 contains useful information extracted from morphology simulation results. It includes the numbers of islands, the nearest distances between islands, the average sizes of spacing, and percolation strength. All the length-related numbers are timed a factor (factor= 1.5) to match from the dimensionless array numbers with real observation from SEM images. In defining the percolation strength, we use the longest cluster in every simulated surface as the percolating chain. It is obvious that percolation strength approaches the coverage for large number of passes because only one large island is left.

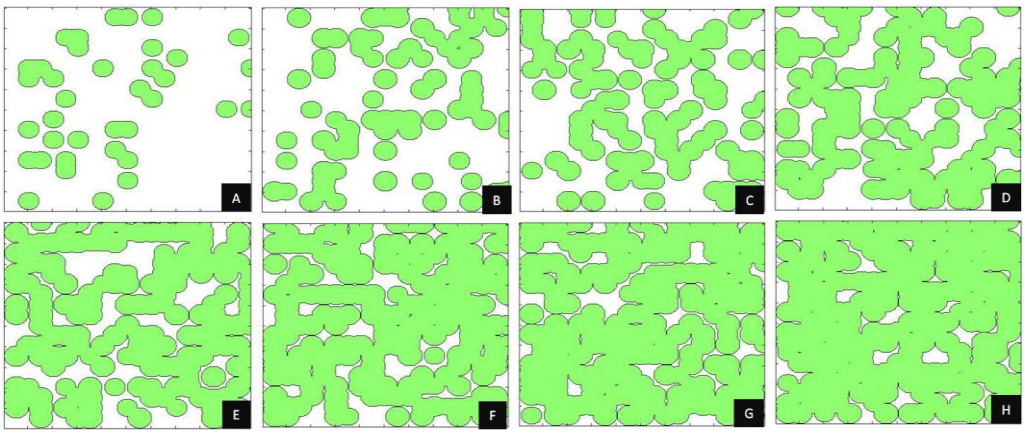

Figure 3.5. Simulated metal surface morphology. From A to H, the number of passes continuously increase from 1 to 8. Green filled areas represent metal; black edges are metal island boundaries.

Table 3.1. Information extracted from morphology simulation results, including coverage, island morphology and percolation strength

Thickness (nm)	Coverage	Number of Islands (/sq)	Distance (nm) (Nearest distance)	Spacing (nm) (hole size)	Percolation Strength
1	0.20	25	13.3	37.5	0.02
2	0.40	30	6.7	45.2	0.06
3	0.53	26	8.7	39.1	0.07
4	0.64	13	7.4	19.5	0.19
5	0.75	9	6.3	13.5	0.58
6	0.83	6	4.9	9.3	0.72
7	0.87	4	1.8	6.2	0.84
8	0.91	2	1.8	3.3	0.90

Simulation results indicate the coverage follows a second order polynomial. The coverage obtained from SEM images and simulated coverage are shown in chapter 2. There is a great match of simulated coverage as p=0.1 and c=0.5 to the coverage from images with respect to embedded Ag thickness. The number of passes matches deposited thickness. In this demonstration, we find the two reasonable parameters to simulate the coverage. Different values of parameters may be needed in discussing different sputtering conditions and materials.

3.3 Resistivity tendency prediction

3.3.1. ZnO/Ag/ZnO

From Han's experimental results [9], we can see a drop in resistivity of 8nm Ag embedded thin film. Unfortunately, a lack of data points makes it difficult to address a continuous curve in describing resistivity change. In Han's discussion, a continuous film appears when Ag thickness reached 14 nm. From percolation view, this means there is a threshold thickness smaller than 14 nm. Our objective is to determine the threshold thickness that percolating Ag layer has a resistivity low enough to dominate the resistivity of the whole sandwiched ZnO/Ag/ZnO.

Simulation results tell us large percolation occurs when Ag thickness increases from 4 nm to 5 nm when percolation strength jumps from 0.19 to 0.58. We can therefore assume the threshold is somewhere between this range. As discussed in introduction of percolation theory, we know the resistivity will be proportional to $(p - p_c)^{-\mu}$. Although each point here has different probability of occupancy, a reasonable use of coverage for both p and p_c eliminates the bias since it exits in both values. Correction factor goes into exponent μ. Therefore, p_c becomes the critical coverage of metal layer; p is the coverage varying with metal layer thickness.

A best fit curve is the solid line presented in figure 3.6. Critical thickness of Ag layer is 4.6 nm where continuous paths form, but an uniform film does not appear until the thickness reaches 14 nm. Exponent μ equals to 3.0. In thickness range from 4.6 nm to 14 nm, percolation phenomenon dominates the metal interlayer morphology. Therefore,

the resistivity drop with respect to Ag thickness mainly follows its relationship with morphology transition. For thickness thinner than 4.6 nm, discontinuous metal layer along with relatively far apart islands remain high resistivity which may mainly depend on the electron ability in tunneling and thermal emission. Percolation phenomenon in this region demonstrates little influence. On the other hand, as the thickness increases over 14 nm where the metal layer is uniform, one can expect another drop in resistivity because uniform film has even lower resistivity. From the observation, the resistivity is approaching to the one of pure metal thin film (10^{-6} Ω cm), but the limitation at around 10^{-4} Ω cm indicates the existence of contact resistance and other effects should be taken into consideration, such as grain boundary scattering and electron mean free path length.

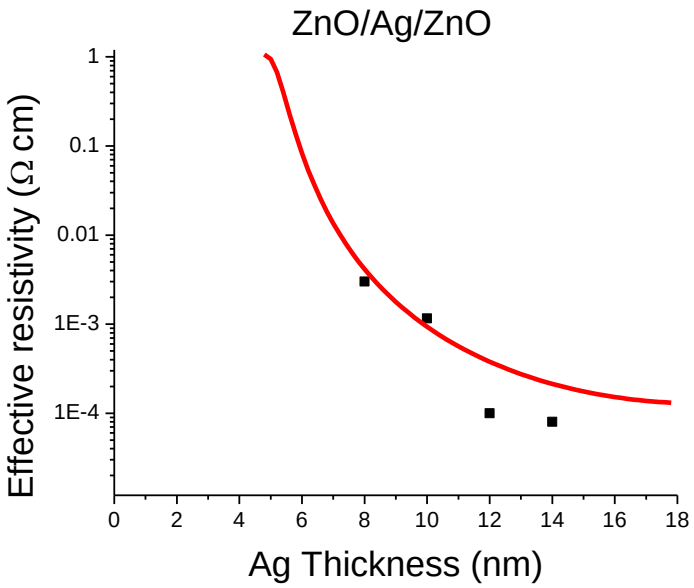

Figure 3.6. Resistivity simulation of ZnO/Ag/ZnO versus the thickness of Ag layer. Red solid line denotes simulation where the coverage change of Ag layer dominates the resistivity change. Black shaded squares (■) are original experimental results.

3.3.2. ZnO/Au/ZnO

Since our model works in Ag case, another application on Au interlayer case will prove the robustness of the model. We now use Sivaramakrishnan's resistivity results on ZnO/Au/ZnO [10] which shows more specific stages transition.

Two parameters in simulation need to be adjusted to simulate the behavior of gold on ZnO surface, especially its wetting ability. Although many studies on Ag and Au nanoparticles have been done [19-21], most of them discussed about adhesion energy of metal on orientated oxides instead of amorphous ones like ZnO from sputtering. However, a quantitative comparison indicates that smaller but better uniform distributed Au particles should be expected. Therefore, we use a little higher p=0.16 and c=0.6 than those in Ag case to simulate Au surface which has more generally distributed small sputtered particles. Figure 3.7. contains Sivaramakrishnan's data points and one solid fitted line which follows $(p - p_c)^{-\mu}$. p_c is the coverage of a 2.6 nm thick Au layer and decay exponent μ here equals to 2.3. This gives us a critical thickness, 2.6 nm, which is the turn point when the resistivity of metal layer starts to dominate. The metal layer becomes uniform as the thickness reaches 7.2 nm.

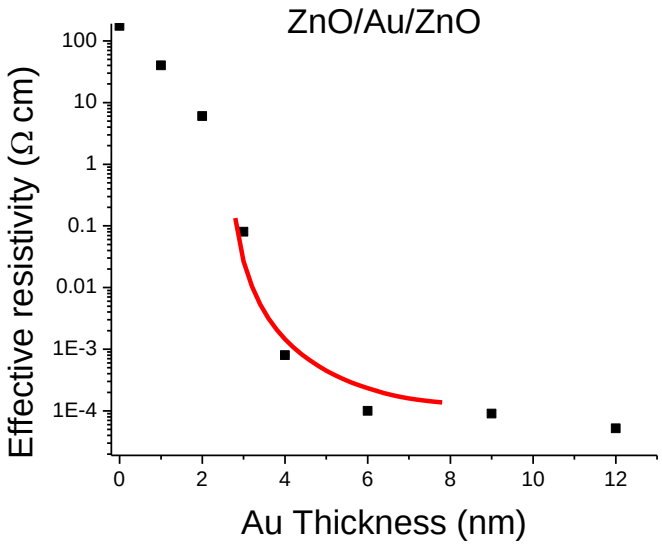

Figure 3.7. Resistivity simulation of ZnO/Au/ZnO versus the thickness of Au layer. Red solid line denotes simulation where the coverage change of Au layer dominates the resistivity change. Black shaded squares (■) are original experimental results.

3.4 Summary

Well fitted curves not only provide us a continuous tendency for easier calculation but also predict the thickness when the morphology largely changes. For ZnO/Ag/ZnO, resistivity starts to drop when Ag is 4.4nm thick, and an uniform film needs to be thicker than 10nm. For ZnO/Au/ZnO, Au middle layer percolates faster and greatly lowers the resistivity with 2.6 nm thickness, and it forms uniformity at 7.2 nm. Since our model can describe electrical behavior properly, a discussion of optical properties with calculation of effective medium coefficient will focus on ZnO/Au/ZnO in next chapter.

Chapter 4: OPTICAL TRANSMITTANCE

4.1 Introduction

High optical transmittance is an important characteristic of transparent conducting oxides. Since our multilayer structures have metal embedded, how does the metal layer behave in terms of optical transmittance becomes an issue in pursuing a highly conductive with good transparency material.

Although bulk metal barely presents transparency especially in visible light region, lights are able to transmit through thin metal films. This characteristic has been widely studied and used as a method to determine the thickness of thin film. However, when the thickness scale goes down to few nanometers, discontinuity has to be taken into consideration [22]. The optical properties of inhomogeneous materials can be described by so-called effective dielectric functions if the wavelength of the probing radiation is much larger than the typical sizes of the inhomogeneities of the system [23]. We therefore define an effective medium which has a matrix material and metal particles to represent the discontinuous metal layer. From the simulation results, we are able to describe the morphology change of metal layers with sputtering time. In the resistivity discussion, percolation behaviors demonstrate their importance in dominating the resistivity of metal layer. Therefore, our optical model will also include a parameter to describe the percolation in discontinuous metal layer.

For future study in plasmon resonance, we would like to focus on noble metals which can result in surface plasmon. Since nice fitted resistivity tendency with percolating surface coverage on ZnO/Au/ZnO samples is demonstrated, we concentrate on simulating optical behaviors of Au embedded multilayer structures. The results will be another support of our percolation simulation.

4.2 Bergman model

Because of the discontinuity of metal layer, we replace a continuous thin film model with an effective medium which contains partial metal in a matrix material. The matrix material here is ZnO. In order to determine effective medium coefficient of discontinuous metal layer, we introduce Bergman representation [24] to calculate transmittance spectra of ZnO/Au/ZnO with respect to different Au thickness.

Bergman presented his calculation on effective dielectric constant of a composite material in 1978 [24]. Depending on the microscopic geometry of material, he defined a set of characteristic geometric functions, whose general analytical properties can be derived. It is also known as the most general form of effective medium approach:

$$\varepsilon_{eff} = \varepsilon_M \left(1 - f \int_0^1 \frac{g(n,f)}{t-n} dn\right), \qquad t = \frac{\varepsilon_M}{\varepsilon_M - \varepsilon} \qquad [24]$$

ε_{eff}, ε_M and ε are the dielectric function of effective medium, matrix material and embedded metal, respectively. A spectral density $g(n,f)$ contains all the morphological details of the microgeometry which are normalized in interval [0,1] for n. *f* is the volume fraction of metal in matrix material. Every microgeometry is represented by a particular

spectral density. However, a continuous spectral density is insufficient to describe the discontinuity of metal layer. A diverging term from continuous spectral density includes percolation strength and δ-function in the form of $g(n,f) = g_0(f)\delta(n) + g_{con}(n,f)$. The g_0 is a function of the volume fraction and the percolation strength. g_{con} describes the continuous terms as for uniform materials. The aim of this function is to describe the discontinuity of embedded metal. The weighting between matrix and metal material will determine the overall optical behaviors of materials.

4.3 Optical transmittance simulation

Transmittance spectra are obtained from the same ZnO/Au/ZnO samples in Sivaramakrishnan's report [10]. Here are fabrication and measurement details. The base pressure prior to deposition was approximately $1x10^{-7}$ Torr. The ZnO was sputtered at 10 mTorr argon pressure using 100 W RF power. Gold was deposited by using 10 mTorr argon pressure and 40 W DC power. There was no break in vacuum at any stage during the preparation of the films. Both top and bottom ZnO layers were approximately 30 nm thick. The Au thicknesses were varied between 1 nm and 12 nm. Schema in figure 3.1a showed the constructions of the stack.

Optical transmittance and reflectivity were measured using an Ocean Optics double channel spectrometer (model DS200) in the wavelength range 300-900 nm with an aluminum mirror as the reference for reflectivity and a bare polyethylene naphthalate (PEN) substrate for transmittance. Tungsten-halogen and deuterium lamps were used for the visible and UV light sources, respectively. All the simulations are done with the help of SCOUT, optical simulation software developed by Dr. W. Theiss [25].

Because the optical behaviors of most materials are sensitive to the fabrication method, we only use the general database for Au which has less variation in refractive index than oxides and polymers. Before fitting Au embedded multilayer structures, we start from fitting the transmittance of bare PEN substrate and bare ZnO on PEN to define their dielectric functions and refractive index.

4.3.1. Bare PEN

An O'Leary-Johnson-Lim (OJL) model and two Kim oscillators [5] are used as the model to identify the dielectric function and the refractive index of PEN. OJL model describes the interband transition, and the two oscillators are expected to the handle possible damping in materials. The experimental and the fitted transmittance of a PEN substrate with 0.125μm thickness is shown in figure 4.1. The deviation is 1.13% which is small enough and suggests the reliability of fitted parameters.

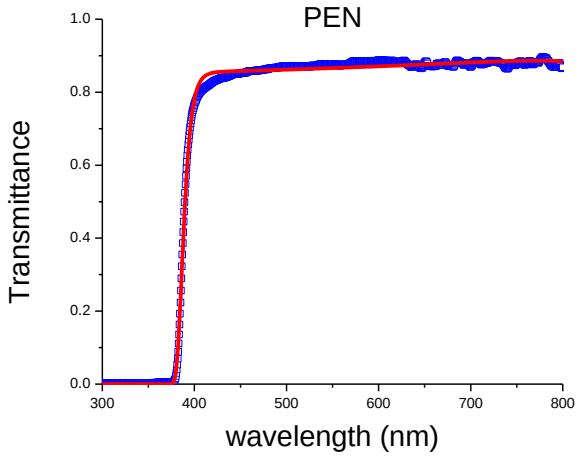

Figure 4.1. Experimental and simulated optical transmittance spectra of bare PEN substrate. Blue open squares (☐) represent experimental observation. Red solid line is fitting curve. Deviation: 1.13%.

4.3.2. ZnO/PEN

We now build a ZnO layer on the top of PEN substrate without any metal layer involved. OJL interband transition model and Drude model are used to describe the ZnO layer. Drude model takes care of possible absorption and damping in ZnO [5]. We identified the thickness of ZnO thin film from Rutherford backscattering spectrometry. In the same sputtering conditions described in chapter 4.1, five minutes sputtering results in a 34 nm ZnO layer. To compare with the metal embedded multilayer structure, we used the transmittance of 68 nm ZnO on PEN for parameter fitting. Figure 4.2 is the fitted spectra. The deviation is 0.49%. It indicates the success in using proper models.

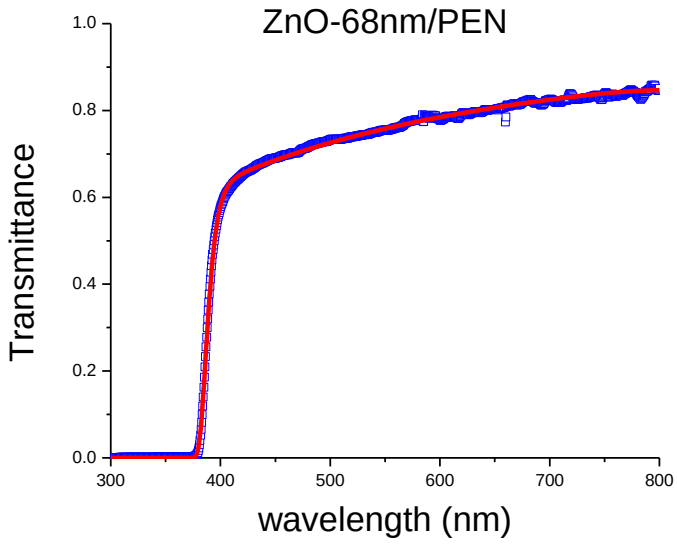

Figure 4.2. Experimental and simulated optical transmittance spectra of 68 nm ZnO thin film on PEN substrate. Blue open squares (☐) represent experimental observation. The red solid line is fitting curve. Deviation: 0.49%.

4.3.3. ZnO/Au/ZnO/PEN

When the metal is involved, we need to consider if it is an uniform thin film or a discontinuous film with percolating clusters. From the resistivity discussion and coverage simulation, we suggested the gold layer starts to dominate the resistivity when the thickness reaches 2.6 nm. An uniform Au layer appears as the thickness reaches 7.2 nm. Basing on these results, we simulate the metal layer with two different models.

For an uniform metal layer, general Au refractive index is extracted from the literature (Johnson & Christy) [26], denoted as Au (JC). For a discontinuous metal layer, we use Bergman representation which contains a matrix material, ZnO, and metal particles, Au, in calculating effective medium coefficients. Figure 4.3 schematically illustrates the structures and models in this two cases.

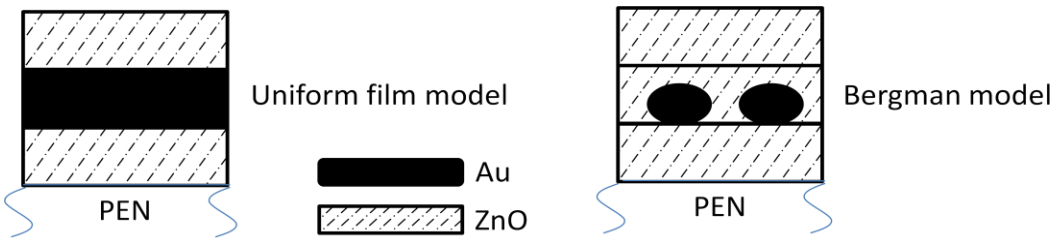

Figure 4.3. Metal layer optical models for two configurations. The middle layer in the left is typically uniform Au thin film and suits for general Au model. In the right, the middle layer contains partial Au particles in ZnO matrix. This combination of two materials is described by Bergman model.

According to our resistivity simulation, for the metal thickness larger than 7.2 nm, the metal layer should be able to perform as an uniform metal layer. Figure 4.4. and 4.5. present experimental observation of 12 nm and 9 nm Au embedded multilayer samples, and along with the fitted spectra which use continuous metal layer model. It can be observed that metallic behaviors dominate Infrared region. Electron damping and scattering at the edge of grain boundary reduce the transmittance in Infrared region. This phenomenon becomes more serious as the thickness of metal layer increases. Good matching between experiment and our simulation validates our model that metal layers are uniform for 12 nm and 9 nm.

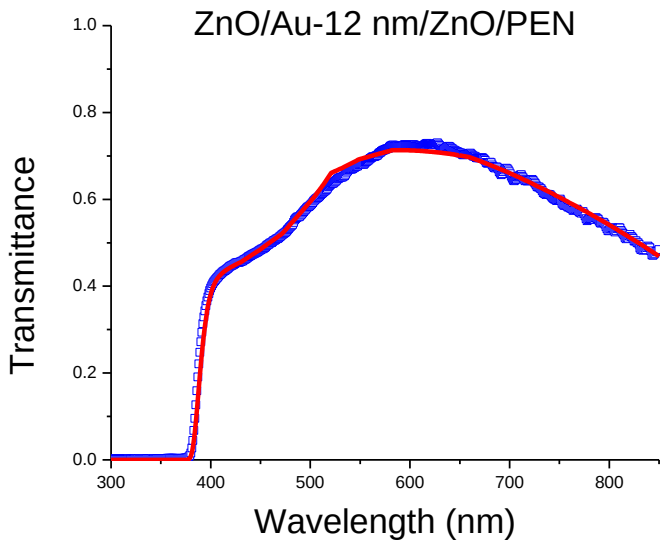

Figure 4.4. Experimental and simulated optical transmittance spectra of 12 nm Au embedded multilayer structure. Blue open squares represent experimental observation. The red solid line is fitting curve. Deviation: 1.21%.

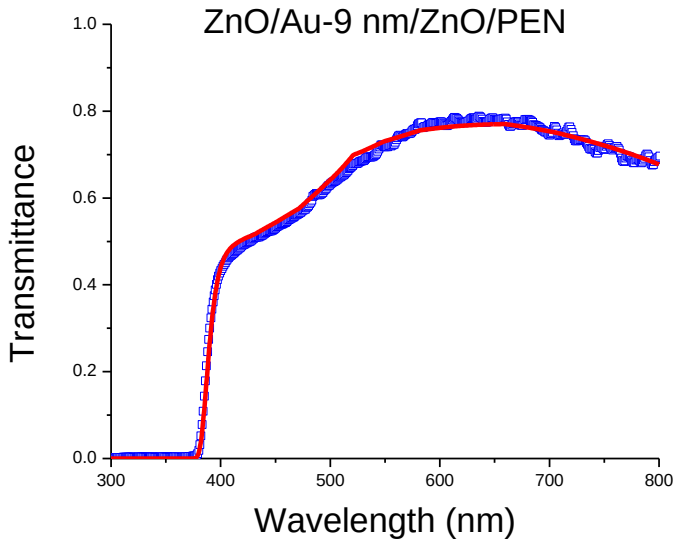

Figure 4.5. Experimental and simulated optical transmittance spectra of 9 nm Au embedded multilayer structure. Blue open squares represent experimental observation. The red solid line is fitting curve. Deviation: 1.49%.

When the metal layer thickness goes down to 6 nm, the uniform metal layer model is not suitable anymore. We migrate to Burgman model. There are three main parameters in using Burgman model: volume fraction, percolation strength and spectral density. Our sputtering pattern simulation can provide exact values for the volume fraction and the percolation strength. Table 4.1 is the volume fraction and percolation strength for 6 nm, 4 nm, 3 nm, 2 nm and 1 nm Au layer.

Table 4.1. Parameters used in Bergman model for each Au layer thickness

Au layer thickness (nm)	Volume Fraction	Percolation Strength
6	0.91	0.91
4	0.78	0.76
3	0.70	0.41
2	0.56	0.06
1	0.27	0.02

By setting spectral density as a free fitting parameter, we obtain relatively good fitting curves for 6 nm to 2 nm. In the 6 nm and 4 nm Au layer thickness, both model results are both presented for comparison. Bergman model provides a smaller deviation in both cases. The deviation drops from 1.57% to 0.37% by using Bergman model. Figure 4.6. to 4.10. present the optical transmittance for 6 nm, 4 nm, 3 nm, 2 nm and 1 nm Au layer, respectively. For 1 nm Au layer, even Bergman model cannot give a good fitting curve. This limitation suggests other factors may be involved. Possible issues are the inaccuracy in determining the metal layer thickness, the limitation of effective medium model and the manual calculation of the coverage.

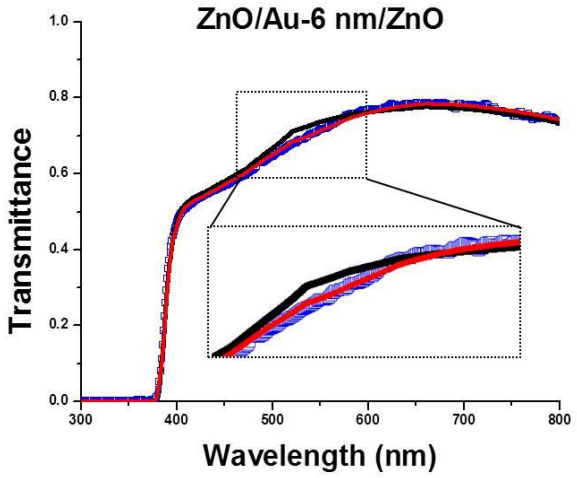

Figure 4.6. Experimental and simulated optical transmittance spectra of 6 nm Au embedded multilayer structure. Blue open squares represent experimental observation. The black solid curve is the fitting curve using uniform Au thin film model. Deviation:1.57%. The red solid line is Bergman fitting curve. Deviation: 0.37%.

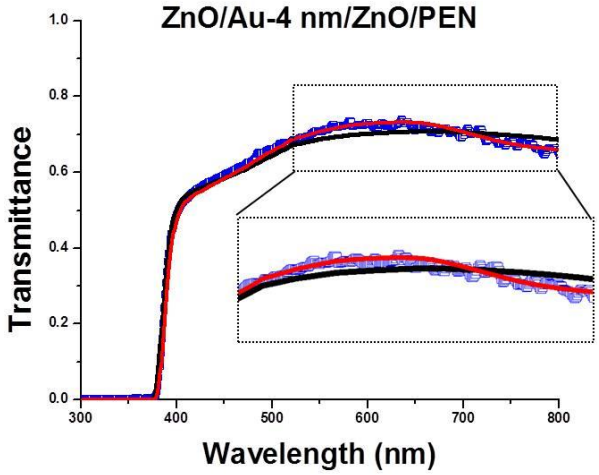

Figure 4.7. Experimental and simulated optical transmittance spectrum of 4 nm Au embedded multilayer structure. Blue open squares represent experimental observation. The black solid curve is the fitting curve using uniform Au thin film model. Deviation: 5.2%. The red solid line is Bergman fitting curve. Deviation: 1.82%.

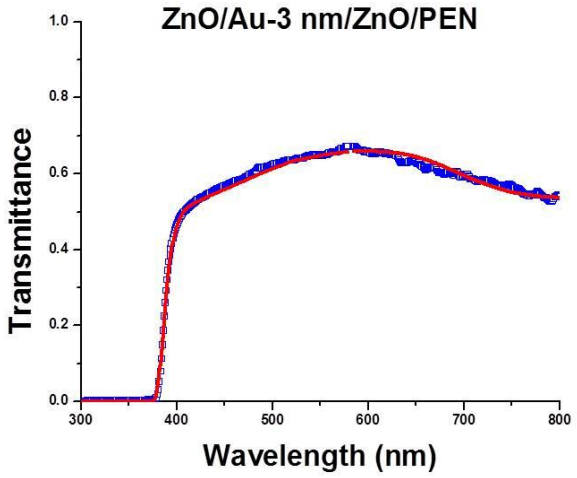

Figure 4.8. Experimental and simulated optical transmittance spectra of 3 nm Au embedded multilayer structure. Blue open squares represent experimental observation. The red solid line is Bergman fitting curve. Deviation: 2.8%.

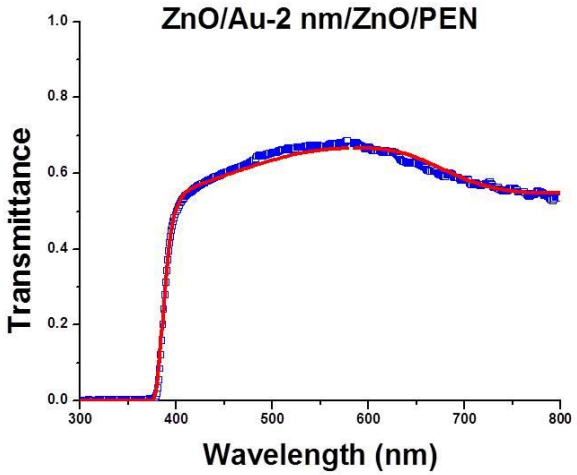

Figure 4.9. Experimental and simulated optical transmittance spectra of 2 nm Au embedded multilayer structure. Blue open squares represent experimental observation. The red solid line is Bergman fitting curve. Deviation: 3.5%.

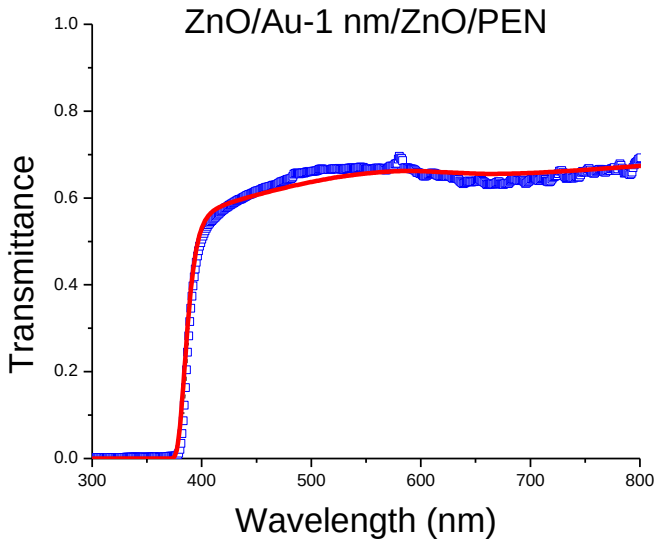

Figure 4.10. Experimental and simulated optical transmittance spectra of 1 nm Au embedded multilayer structure. Blue open squares represent experimental observation. The red solid line is Bergman fitting curve. Deviation: 4.4%.

4.4 Summary

In this chapter, optical transmittance simulation demonstrates good coherence with the previous resistivity discussion. When the metal thickness is smaller than 2 nm, the metal layer has low a volume fraction and percolation strength. As expected, for metal thickness larger than 2 nm, the metal layer dominates optical behaviors: transmittance decreases with Au thickness increase in long wavelength region due to more electron scatterings and the short wavelength absorption due to the electron interband transition. The continuous metal layer model does not fit for thickness smaller than 6 nm which supports previous conclusion that the metal layer is discontinuous in this thickness. By using effective medium model, good matches between the observation and the simulation are obtained.

Chapter 5: CONCLUSION

From the morphology simulation and the real surface observation, a phenomena similar to percolation is observed. Based on simulation results, we are able to use the coverage as a known parameter for data fitting. Three growth stages of the metal layer are proposed including islands only stage, percolating stage and uniform thin film stage. For islands only in metal layer, resistivity remains high since islands are far apart and not able to largely reduce resistivity. However, in second stage, good consistence between the experimental observation and percolation theory implies that metal layer is percolating as the thickness increases. Islands form conductive paths during this stage, but part of metal may remain isolated or only form short conductive paths. Therefore, the resistivity decreases. Finally, the metal layer becomes an uniformly thin film and performs dramatically reduction in resistivity which is close to the resistivity of metal.

Another proof supporting the transition from percolating films to uniform thin films is the optical behavior. We use the effective medium model to calculate the overall optical behaviors for discontinuous films, and simulation results are well consistent with the observation in this model. This indicates the parameters in effective medium model are trustable which include the volume fraction and percolation strength defined from morphology simulation.

Since we are pursuing a low resistivity and high transparency material, a figure of merit (FOM) is defined as transmittance divided by sheet resistance. Higher FOM indicates the material has better performance. To emphasize on resistivity performance, Haacke [27] proposed that the transmittance should be multiplied by 10 times. We have estimated the Haacke figure of merit, φ_{TC}, for the transparent conducting films as follows:

$$\varphi_{TC} = \frac{T_{av}^{10}}{R_{sh}} \qquad [27]$$

where T_{av} is the average transmittance and R_{sh} is the sheet resistance. For our interests in solar cell applications, T_{av} is weighted with respect to solar irradiance at sea level [28]. We use Haacke figure of merit to identify the optimal metal thickness in ZnO/Au/ZnO case. The variation of FOM is also presented in figure 5.1. It can be seen that the largest FOM appears with 9 nm Au interlayer which just reaches the uniform thin film thickness. Further increase in metal layer thickness makes decrease in transmittance. Table 5.1. contains Haacke FOM for different metal interlayer thicknesses. It should be noticed that even 7 nm metal interlayer has higher transmittance in near infrared region, but its FOM is smaller than the one with 6 nm interlayer. This is because 7nm metal interlayer has better light transmittance in infrared wavelength, but the atmosphere absorbs more lights in that region. The advantage of the 7 nm interlayer is not demonstrated with solar spectrum.

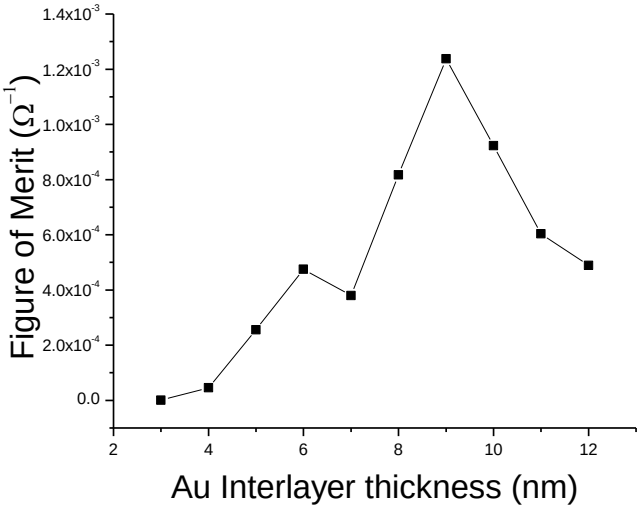

Figure 5.1. Haacke figure of merit with respect to Au interlayer thickness. Exact value of each point is provided in table 5.1.

Table 5.1. Values of Haacke figure of merit with respect to metal interlayer thickness.

Metal Interlayer Thickness (nm)	Haacke Figure of Merit (Ω^{-1})
3	7.61×10^{-7}
4	4.56×10^{-5}
5	2.56×10^{-4}
6	4.75×10^{-4}
7	3.80×10^{-4}
8	8.17×10^{-4}
9	1.24×10^{-3}
12	4.89×10^{-4}

The coherence of resistivity and optical transmittance validates the simulation of the sputtered pattern and the incorporation of percolation theory. Instead of using data points, we obtain relatively continuous variation of resistivity and optical transmittance. We are able to describe and predict material properties without depending on experimental results which may be insufficient in describing whole property transition.

The models and simulation in this work can be improved by considering more details of the morphology transformation depending on interested topics or different sputtering rates. By inserting different parameters into the simulation, one is able to apply the results on different materials. Basing on the understanding of metal layer morphology, the criteria for generating surface plasmon which strongly depends on metal island size can be well studied as a future topic. Further improvement on similar material structures can also be reached.

REFERENCES

[1] M. Katayama, "TFT-LCD Technology", *Thin Solid Films* **341** (1999): 140-147.

[2] T. Minami, "Transparent conducting oxide semiconductors for transparent electrodes", *Semicond. Sci. Technol.* **20** (2005): S35-S44.

[3] C. G. Granqvist, "Transparent conductors as solar energy materials: A panoramic review", *Solar Energy Materials & Solar Cells* **91** (2007): 1529-1598.

[4] H. Hosono, "Recent progress in transparent oxide semiconductors: Materials and device application", *Thin Solid Films* **515** (2007): 6000-6014.

[5] M. Fahland, T. Vogt, W. Schoenberger and N. Schiller, "Optical properties of metal based transparent electrodes on polymer films", *Thin Solid Films* **516** (2008): 5777-5780.

[6] C. Guillen and J. Herrero, "TCO/metal/TCO structures for energy and flexible electronics", *Thin Solid Films* **520** (2011): 1-17.

[7] Y. Park, KH Choi and HK Kim, "Room temperature flexible and transparent ITO/Ag/ITO electrode grown on flexile PES substrate by continuous roll-to-roll sputtering for flexible organic photovoltaics", *J. Phys. D: Appl. Phys.* **42** (2009): 235109-235116.

[8] M. Chakaroun, B. Lucas, B. Ratier, C. Defranoux, J.P. Piel and M. Aldissi, "High quality transparent conductive electrodes in organic photovoltaic devices", *Thin Solid Films* **518** (2009): 1250.

[9] H. Han, N. D. Theodore and T. L. Alford, "Improved conductivity and mechanism of carrier transport in zinc oxide with embedded silver layer", *Journal of Applied Physics* **103** (2008): 013708.

[10] K. Sivaramakrishnan and T. L. Alford, "Conduction and transmission analysis in gold nanolayers embedded in zinc oxide for flexible electronics", *Applied Physics Letters* **96** (2010): 201109.

[11] S. Norrman, T. Andersson and C. G. Granqvist, "Optical properties of discontinuous gold films", *Physical Review B* **18** 2 (1978): 674-695.

[12] D. Zhang, H. Yabe, E. Akita, P. Wang, R. Murakami and X Song, "Effect of silver evolution on conductivity and transmittance of ZnO/Ag thin films", *Journal of Applied Physics* **109** (2011): 104318.

[13] P. Wang, D. Zhang, D. H. Kim, Z. Qiu, L. Gao, R. Murakami and X. Song, "Enhancement of light transmission by coupling to surface Plasmon polaritons of a layer-plus-islands silver layer", *Journal of Applied Physics* **106** (2009) 103104.

[14] T. W. Ebbesen, H. J. Lezec, H. F. Ghaemi, T. Thio and P. A. Wolff, "Extraordinary optical transmission through sub-wavelength hole arrays", *Nature* **391** (1998): 667-669.

[15] H. Wei and H. Eilers, "From silver nanoparticles to thin films: Evolution of microstructure and electrical conduction on glass substrates", *Journal of Physics and Chemistry of Solids* **70** (2009): 459-465.

[16] Y. Suzuki, Y. Ojima, Y. Fukui, H. Fazyia and K. Sagisaka, "Post-annealing temperature dependence of infrared absorption enhancement of polymer on evaporated silver films", *Thin Solid Films* **515** (2007): 3073-3078.

[17] K. Sieradzki, K. Bailey and T. L. Alford, "Agglomeration and percolation conductivity", *Applied Physics Letters* **79** 21 (2001): 3401.

[18] B. J. Last and D. J. Thouless, "Percolation theory and electrical conductivity", *Physical Review Letters* **27** 25 (1971): 1719-1721.

[19] Dietrich Stauffer and Amnon Aharony, *Introduction to percolation theory*, (London, Washington D.C. : Taylor & Francis, 1992).

[20] S. Joo and D. F. Baldwin, "Adhesion mechanisms of nanoparticle silver to substrate materials: identification", *Nanotechnology* **21**(2010): 055204.

[21] B. Medasani, Y. H. Park and I. Vasiliev, " Theoretical study of the surface energy, stress, and lattice contraction of silver nanoparticles", *Physical Review B* **75** (2007): 235436.

[22] K. K. Nanda, A. Maisels and F. E. Kruis, "Surface tension and sintering of free gold nanoparticles, *J. Phys. Chem. C* **112** (2008): 13488-13491.

[23] A. Patra, V. Damodara Das and S. Kasiviswanathan, "Optical and photoluminescence studies of gold nanoparticles embedded ZnO thin films", *Thin Solid Films* **518** (2009) 1399-1401.

[24] W. Theiss, "The use of effective medium theories in optical spectroscopy", *Festkörperprobleme* **33** (1994) 149.

[25] D. J. Bergman, "The dielectric constant of a composite material- A problem in classical physics", *Physics Reports* **43** (1978): 377-407.

[26] SCOUT Tutorial by W. Theiss Hard- and Software company.

[27] PB Johnson, “Optical constants of Ag, Au, and Cu thin films”, *Bulletin of the American Physical Society* **16** 7 (1971): 785.

[28] G. Haacke, “New figure of merit for transparent conductors”, *Journal of Applied Physics* **47** (1976): 4086.

[29] A. Mecherikunnel and C. H. Duncan, “Total and spectral solar irradiance measured at ground surface”, *Appled Optics* **21** 3 (1982): 554.